



HAL
open science

Freeze-thaw resistance of limestone roofing tiles assessed through impulse vibration monitoring and finite element modeling in relation to their microstructure

Yannick Igor Fogue-Djombou, Stéphane Corn, Laurent Clerc, David Salze,
Eric Garcia-Diaz

► To cite this version:

Yannick Igor Fogue-Djombou, Stéphane Corn, Laurent Clerc, David Salze, Eric Garcia-Diaz. Freeze-thaw resistance of limestone roofing tiles assessed through impulse vibration monitoring and finite element modeling in relation to their microstructure. *Construction and Building Materials*, 2019, 205, pp.656-667. 10.1016/j.conbuildmat.2019.01.211 . hal-02424972

HAL Id: hal-02424972

<https://hal.science/hal-02424972>

Submitted on 22 Oct 2021

HAL is a multi-disciplinary open access archive for the deposit and dissemination of scientific research documents, whether they are published or not. The documents may come from teaching and research institutions in France or abroad, or from public or private research centers.

L'archive ouverte pluridisciplinaire **HAL**, est destinée au dépôt et à la diffusion de documents scientifiques de niveau recherche, publiés ou non, émanant des établissements d'enseignement et de recherche français ou étrangers, des laboratoires publics ou privés.



Distributed under a Creative Commons Attribution - NonCommercial 4.0 International License

1 **Title:** Freeze-thaw resistance of limestone roofing tiles assessed through
2 impulse vibration monitoring and finite element modeling in relation to their
3 microstructure

4 **Authors:** Yannick Igor FOGUE DJOMBOU^{a,b}, Stéphane CORN^a, Laurent CLERC^a, David SALZE^b,
5 Eric GARCIA-DIAZ^a

6 **Corresponding author:** Stéphane CORN^a stephane.corn@mines-ales.fr

7 ^aC2MA, IMT Mines Alès, Université de Montpellier, 6 avenue de Clavières, 30319, Alès
8 Cedex, France

9 ^bLGEI, IMT Mines Alès, Université de Montpellier, 6 avenue de Clavières, 30319, Alès Cedex,
10 France

11 **Keywords:**

12 Freeze-thaw, damage, vibration, limestone roofing tiles, vernacular building
13 material, architectural heritage, finite element modeling

14
15 **Abstract:**

16 Stone slate used for roofing is often considered as a key element of architectural heritage,
17 especially in the French “Massif Central” region, where it contributes to the Mediterranean
18 agropastoral cultural landscape of the “Causses and Cévennes” perimeter registered on the
19 UNESCO World Heritage List. This material is subjected in service to severe and cycled
20 climatic conditions (freeze-thaw) that may lead from mechanical damage to failure and thus
21 compromise its use. In this paper, a damage assessment strategy of limestone roofing tiles
22 samples during freeze-thaw cycles, based on the monitoring of their impulse vibration
23 response, is proposed. Variations of the modal parameters such as resonant frequencies,
24 damping ratios and mode shapes are analyzed through a 3D finite element model of
25 each sample. This allows quantifying the loss of dynamic stiffness due to the ongoing damage
26 and drawing comparisons between the studied materials in relation to their microstructural and
27 mesostructural damages. Thus presence of pre-existing diagenetic features, such as stylolites
28 (Ds in Nicholson classification), in limestone tiles with unimodal micropore, or with
29 presence of high porosity volume, constitute weaknesses of the stone that can lead to damage.

30

31 1. **Introduction:**

32 Flagstone or tilestone[1] (figure 1) is a natural stone material, splits along horizontal lines of
33 weakness of stone, that can be used for roofing. This material is either metamorphic rock
34 (slates[2]), sedimentary rock (sandstone, limestone or volcanic tuffs[1,3,4]), or magmatic rock
35 (Clinkstone). Tilestones are used for roofing in many regions in Europe (France, Italy, Spain,
36 Great Britain[2,5]) and contribute to the authenticity of a region, such as in the Massif Central
37 area in France, where they constitute a key element of the Mediterranean agropastoral cultural
38 landscape of the “Causses and Cévennes” perimeter registered on the UNESCO World
39 Heritage List. Limestone tilestone subjected to aggressive climatic conditions could undergo
40 mechanical damage, compromising its roof sealing function. The freeze–thaw cycle protocol,
41 which is conducive to simulate such aggressive environmental conditions, has often been used
42 to study the behavior of limestone used in building heritage [6,7].



48 **Figure 1** Limestone tilestone from Causse Larzac (Aveyron - France)

49 In sedimentology, limestone of stratum formation results from cyclicity changes
50 insedimentary deposition conditions, inducing either a change in sediment input rate,
51 sediment composition, or alternation in the sedimentation and non-sedimentation phases[4].
52 « Plattenkalk » is the name used in the literature to describe a type of tilestone as being
53 sequences of fine-grained, laminated limestones, bedded in centimeter-decimeter
54 thickness[4,8]. The studyof limestone tilestone structure must consider(1) boundary bedding
55 surfaces, (2) bedthickness, (3) composition and internal structure ofbeds or core tilestone
56 surfaces, (2) bedthickness, (3) composition and internal structure ofbeds or core tilestone

57 (figure 2): boundary bedding surfaces (upper and lower surfaces of beds) are caused by abrupt
58 changes in depositional conditions, non-deposition or erosion. However, these bedding planes
59 also result from diagenetic processes or weathering[8]. Bed thickness of limestone tilestone
60 can range from about three to eight centimeters. Composition and internal structure of beds
61 (core tilestone) depend on sedimentary diagenetic process[4,8]. Differences between
62 diagenetic processes could lead to different pre-existing diagenetic features characteristic of
63 core tilestone. These pre-existing diagenetic features, coupled with rock strength and textural
64 properties, have been shown to have an influence on the deterioration mode of limestone
65 subject to freeze-thaw cycles[9]. In fact, while some pre-existing diagenetic features such as
66 syndepositional deformation structures do not appear to influence breakdown, others such as
67 incipient fractures, cavities and minor lithological boundaries frequently coincide with
68 concentrations of deterioration[9]. We will adopt the classification of pre-existing diagenetic
69 features presented as “flaws” by Nicholson[9] to characterize the pre-existing diagenetic
70 features of the limestone tilestones that will be used in this study (figure 2).

71

72 [Figure 2 Structure of limestone tilestone and classification of pre-existing rock diagenetic features observed at the](#)
73 [material scale \[9\]](#)

74 In addition to the influence of pre-existing diagenetic features on the deterioration process of
75 limestone subject to freeze-thaw cycles, previous work of others focused on further stone
76 physical parameters, such as the importance of the degree of saturation. In literature, a ratio of
77 80% [10] or 70% [11] of the degree of saturation is proposed as a critical degree of saturation
78 and beyond that threshold the material is damaged by frost. The porous network
79 characteristics such as the distribution of pore size, is also a physical parameter that influences
80 deterioration of limestone subject to freeze-thaw cycles. In fact, Bellanger [12] proposes that
81 grainstone, with a bimodal porosity, a low degree of saturation and a high volume of trapped
82 air, is more resistant to frost than mudstone facies which has an unimodal, well-connected
83 pore network, a high degree of saturation and a low volume of trapped air [12]. The influence
84 of the mechanical parameters like Young's modulus and transfer parameters like permeability
85 is also investigated. Saad [13] found that rocks with high permeability and low young
86 modulus Young's modulus are more frost resistant than rocks with low permeability and high
87 Young's modulus. And more recently, Eslami [7] studied the influence of physical and
88 mechanical properties on the durability of limestone subjected to freeze-thaw cycles. Indeed,
89 in this study the authors have proposed the possibility to predict frost damage of limestone
90 from the ratio of the volume fraction of water to that of air rather than from only the total
91 porosity or degree of saturation [7]. In most cases, non-destructive methods based on
92 monitoring of wave velocity are used to monitor damage to the limestone subject to freeze-
93 thaw [6,7,15]. But Saad [16] has shown that although the vibration method and the ultrasonic
94 method are two equivalent methods to characterize the damage [17,18], the vibration method
95 is more suitable for monitoring limestone subject to freeze-thaw cycles, because it is more
96 sensitive to structural changes than the ultrasonic method [13,19]. In reference [13] some
97 limits of the use of resonant frequency measurement were presented, such as the impossibility
98 to discriminate two similar rocks with different frost damage sensitivities, or the inefficiency
99 of the use of damping parameters for monitoring damage. Vibration damage monitoring is

100 frequently used in the field of damage monitoring of concrete subject to freeze-thaw cycles
101 [20–22]. In particular Lund [22] used Operational Modal Analysis (OMA)[23] to assess the
102 damage of pervious concrete subject to freeze-thaw cycles. In this case, all frequencies shown
103 the same decay during the weathering process. In the case of natural stones, because of the
104 heterogeneity and the anisotropy of the material (pre-existing or induced by the weathering
105 process), eigenmodes and frequencies could exhibit a different sensitivity to damage severity.
106 Damping ratio is not often used to monitor weathering of limestone or concrete subjected to
107 freeze-thaw cycles. As it is related on[24], the use of damping ratio on the assessment of
108 damage in a structure has many advantages, such as being more sensitive than frequency
109 to damage [25] or in some cases, while the crack is undetectable on frequency, it is although
110 possible to measure an increase in the damping ratio[26].

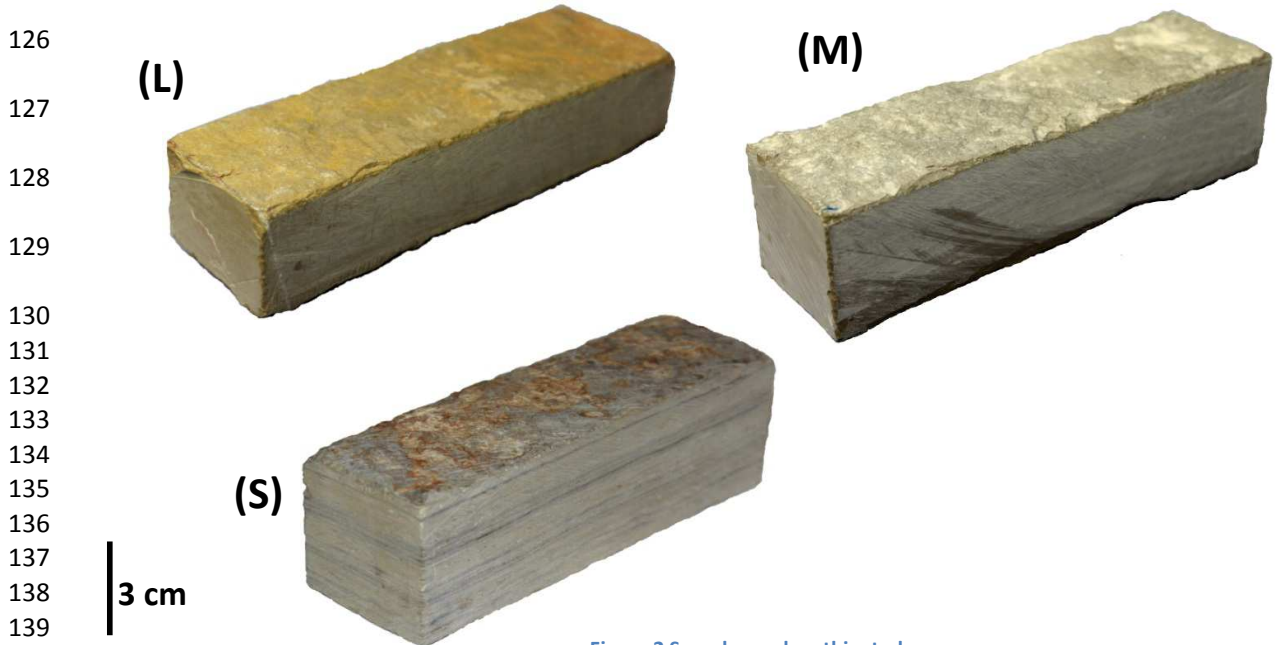
111 The purpose of the present work was to monitor the impulse vibration response of several
112 limestone samples during freeze-thaw cycles and to compare this response to the
113 structure damage observed at mesoscale and microscale. The first part will concern the
114 sensitivity on frequency and damping ratio during freeze-thaw cycles. Then, a correlation
115 between the vibration response and the damage process at microscale and mesoscale will be
116 made. We will conclude by investigating the implications in terms of mechanical properties of
117 our structures, by assessing the Young's modulus through a FE model updating technique on
118 the basis of the experimental natural frequency measurements.

119 **2. Materials and Methods:**

120 **2.1. Characteristics of studied stones:**

121 Limestone samples were taken from the three active quarries of Montdardier, Laval-
122 du-Tarn and Saucière, located in the departments of Gard, Lozère and Aveyron (in the
123 southern area of the Massif Central region of France). Three parallelepiped samples were cut

124 from each selected tilestone (Laval-du-Tarn (L) = L1, L2, L3; Montdardier (M) = M1, M2,
 125 M3; Sauclière (S) = S1, S2, S3) for the freeze-thaw cycle. (Figure 3)



141

Rocks origin	Laval-du-Tarn (L)			Montdardier (M)			Sauclière (S)		
Samples name	L1	L2	L3	M1	M2	M3	S1	S2	S3
Length (mm)	156,6	156,6	156,6	160,3	160,3	160,3	135,23	135,13	135,15
Width (mm)	45,25	50,5	46,6	44,4	43,3	45,2	41	38	41,53
Thickness (mm)	32,13	29,5	32,28	41,3	36,9	38,33	43,48	42,4	42,75

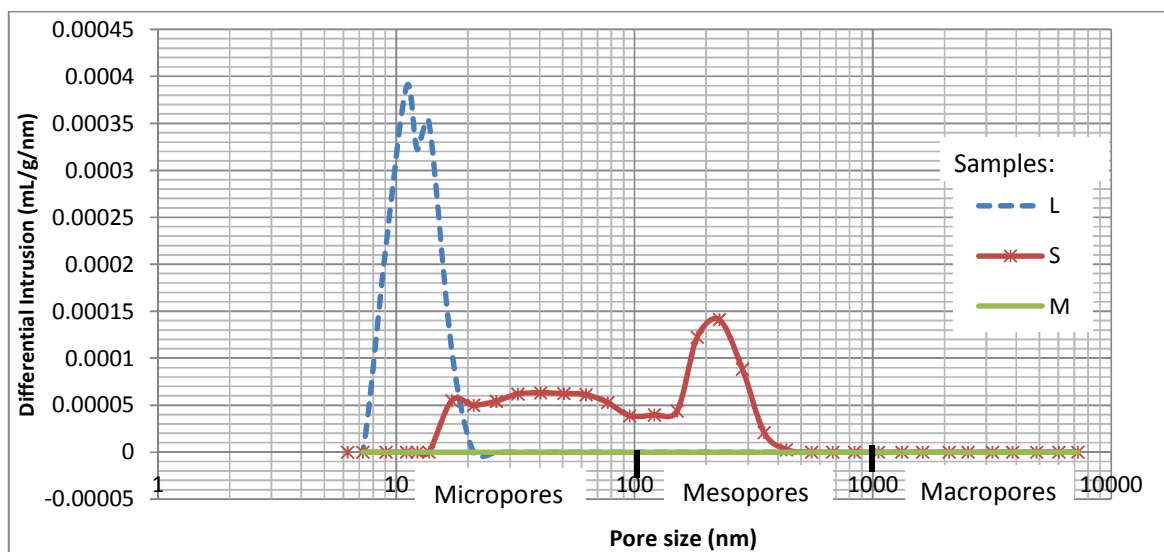
142
 143
 144
 145
 146
 147 Table 1: dimensions of samples

148
 149 Samples L and M are micritic limestone [27] made of 97% of calcite and Sample S is Gray
 150 dolomite with varying facies and sedimentary figures[28]. These stones have been chosen
 151 firstly because they are quarried from the last remaining active quarries that produce-
 152 limestone tilestone in France that has been widely used in the construction of vernacular and
 153 heritage architecture in the Massif Central (Table 2), and secondly because they present
 154 classic diagenetic features often observed in this sedimentary stone at the material scale
 155 according to the Nicholson classification[9]. In fact, from an optical microscope observation
 156 of a polished section of these samples, it is possible to distinguish diagenetic features such as
 157 **Of**= primary diagenetic features(O) with shell fragments(f), **Ds**= diagenetic and metamorphic
 158 effect(D) with stylolites and pressure solution features(s); **Dv**= diagenetic and metamorphic

159 effect with mineral veins and healed fractures; **Wb**= weathering effects(W) with banding (b);
 160 **Sl**=primary depositional structure (S) with laminations (l); **Lm**= lithological variations (L)
 161 with variations in mineralogical composition (m); **Lt**= lithological variations (L) with
 162 truncated surface (table2).

163 **2.2. Porous characteristics:**

164 The mercury porosimetry was carried out in Micromeritics'AutoPore IV 9500 Series Mercury
 165 Porosimeters and was performed on two fragments for each stone to investigate the pore size
 166 distribution. The water porosities was measured, to determine the open porosity N_o and total
 167 porosity N_t , according to the NF EN 1936standard [29]. The water absorption at atmospheric
 168 pressure was measured to assess the saturation rate after 48 hours, according to the NF EN
 169 13755standard. Table 2 summarizes these physical properties. Stone L and M are very low
 170 porous material with unimodal porous networks consisting essentially of micropores (about
 171 13 nanometers for sample L and less than 7 nanometers for sample M since there was no
 172 intrusion of mercury during the test (figure 4). Whereas stone S is a more porous media with a
 173 bimodal porous network, and consists of a majority of mesoporous (between 100 nm and
 174 1000 nm) and a few parts of micropore (figure 4).



175
 176 **Figure 4 Pore size distribution curves of the studied limestones**



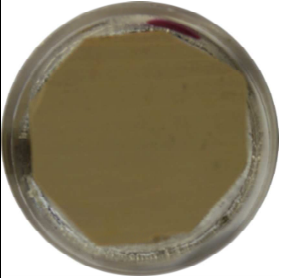



Tilestone (origin)	Age	Polished section	Nicholson pre-existing diagenetic features classification	Total porosity Nt (%)	Open porosity No (%)	Saturation rate S48h (%)	Porous networks (mean pore diameter)	Density (g/cm ³)	Bending strength (MPa)	Example of construction
Laval-du-Tarn (Lozère-France)	Oxfordian		Of, Ds, Dv, Wb	2,90	1,81	56	Unimodal (13 nm)	2,65	25	Farm (Saint-andre-de-vezines - Aveyron-France) 
Montdardier (Gard-France)	Oxfordian		Of, Wb	3,44	1,75	48	Unimodal (<7 nm)	2,63	22	Bread oven (Saint-andre-de-vezines- Aveyron-France) 
Sauclière (Aveyron-France)	Lotharingian		Sl, Lm, Lt, Of, Ds	11,99	10,8	60	Bimodal (105 nm)	2,51	26	Tour du vialas du pas de Jaux (Vilas-du-pas-de-jaux-Aveyron-France) 

Table 2: Characteristics of selected limestone tilestone, with their sedimentary features according to the classification of Nicholson [9]: **Of**= primary diagenetic features(O) with shell fragments(f), **Ds**= Diagenetic and metamorphic effect(D) with stylolites and pressure solution features(s); **Dv**= Diagenetic and metamorphic effect with mineral veins and healed fractures; **Wb**= Weathering Effects(W) with banding (b); **Sl**=Primary Depositional Structure (S) with laminations (l); **Lm**= Lithological Variations (L) with variations in mineralogical composition (m); **Lt**= Lithological Variations (L) with truncated surface.

177 **2.3. Freeze-thaw test:**

178 Freeze–thaw testing for this study was carried out in a Dycometal freezing chamber (model
179 CHD - 525). Before beginning the cycle, all the samples were saturated by immersing them
180 for 48 hours at 20°C. The test was performed so as to be harsher than EN 12371 standard used
181 for natural stone[30] and consists of four parts: (1) decrease of temperature in chamber from
182 20°C to -30°C for 30minutes without water, (2) constant temperature in chamber gel at -30°C
183 for 1.5 hours, (3) increase of temperature in chamber from -30°C to 10°C for 30minutes, (4)
184 constant temperature thaw in chamber at 10°C for 1.5 hours under water. Thawing is done
185 under water in order to keep the ratio of water constant in the sample. After the first ten
186 cycles, and every 20 cycles, samples are removed from the freezing chamber so as to monitor
187 the damage with vibration response measurement and to analyze of the microstructure.

188 **2.4. Damage monitoring:**

189 *Test setup for vibration response acquisition*

190 A Kistler instrumented hammer was used to impact the sample so as to produce vibration of
191 the structure. From a Kistler accelerometer sensor installed on the sample, the transient
192 response is acquired with a National Instruments (NI) acquisition system (USB-4431) and the
193 corresponding Frequency Response Function (FRF) is computedthrough an FFT
194 algorithmembedded in ModalViewsoftware.Specimens are "suspended" by using soft foam
195 supports, which allows considering free-free boundary conditions of the beam in the ongoing
196 eigenparameters calculations [31](Figure 5).

197

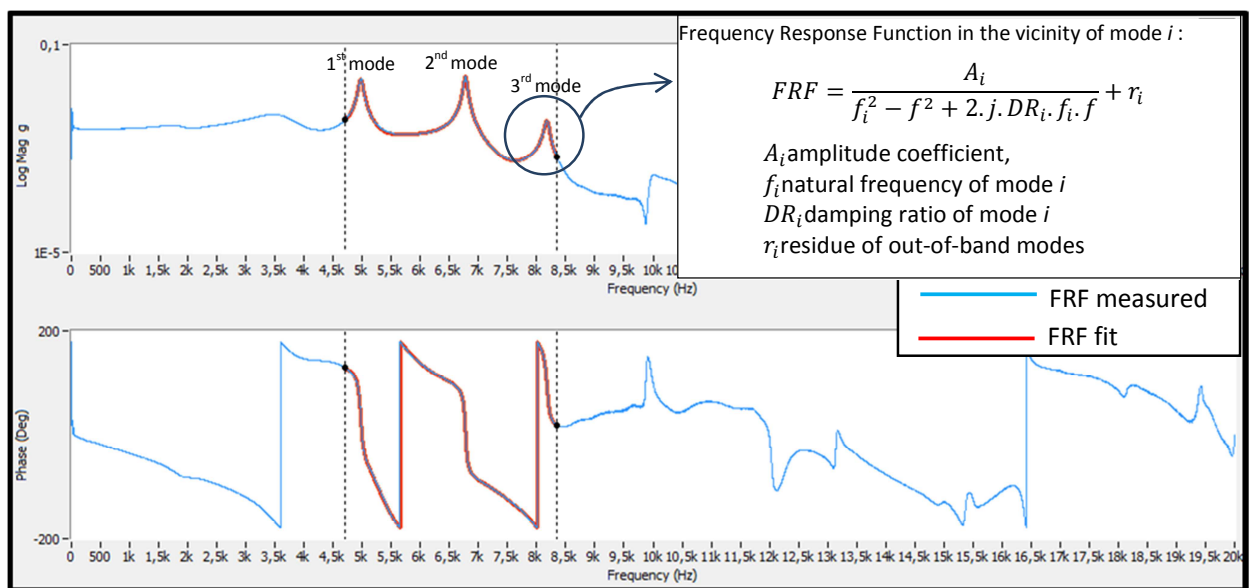
198

199

200 **Figure 3 Test setup used for modal analysis**

201 *Extraction of modals parameters*

202 Modal analysis is performed by using the curve fitting of FRF technique available in the
203 ModalView Software. Curve fitting technique basically consists in interpolating the
204 measurement points of the FRF in the vicinity of each frequency peak (figure 6) with a
205 parameterized function of the damped vibration response of a single-dof model [32]. From the
206 FRF fit, the natural frequencies ($f_i(n)$) and the damping ratio ($DR_i(n)$) of mode i are extracted
207 and monitored for the first three modes after each sequence of n cycles [32,33].



208

209 **Figure 6 Measured FRF and curve fitting in ModalView software**

210 *Vibration damage monitoring parameters*

211 After every n cycle, the Relative dynamic elastic modulus for each mode i (RDEM_i(n))[22]
212 and Damping Ratio (DR_i(n)) are calculated to assess the loss of stiffness and thus the
213 deterioration rate of the specimens under freezing and thawing at n cycles. The RDEM_i(n) of
214 the specimen is determined with the following formula (1) and (DR_i(n)) is obtained from the
215 extracted modal parameters.

216
$$\text{RDEM}_i(n) = \left(\frac{f_i^2(n)}{f_i^2(0)} \right) \times 100 (\%) \quad (1)$$

217 Where,

218 $f_i(n)$ = natural frequency of mode i after n cycles of freezing and thawing;

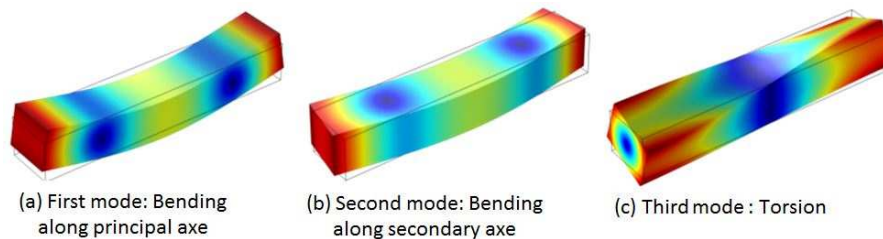
219 $f_i(0)$ = initial natural frequency of mode i.

220 *Microstructure damage assessment:*

221 For the microstructural investigations, pieces of cylindrical polished samples of 3 cm of
222 diameter were examined using a Quanta 200 FEG SEM from FEI coupled to an Oxford INCA
223 X-ray energy dispersive X-ray spectroscopy (EDX) analyzer. An optical microscopy
224 observation has also been investigated on polished section of these materials before and after
225 freeze-thaw cycles, especially on the zone where the damage occurred, so as to characterize
226 weathering on a mesoscale and microscale.

227 *Elastic coefficients evaluation technique:*

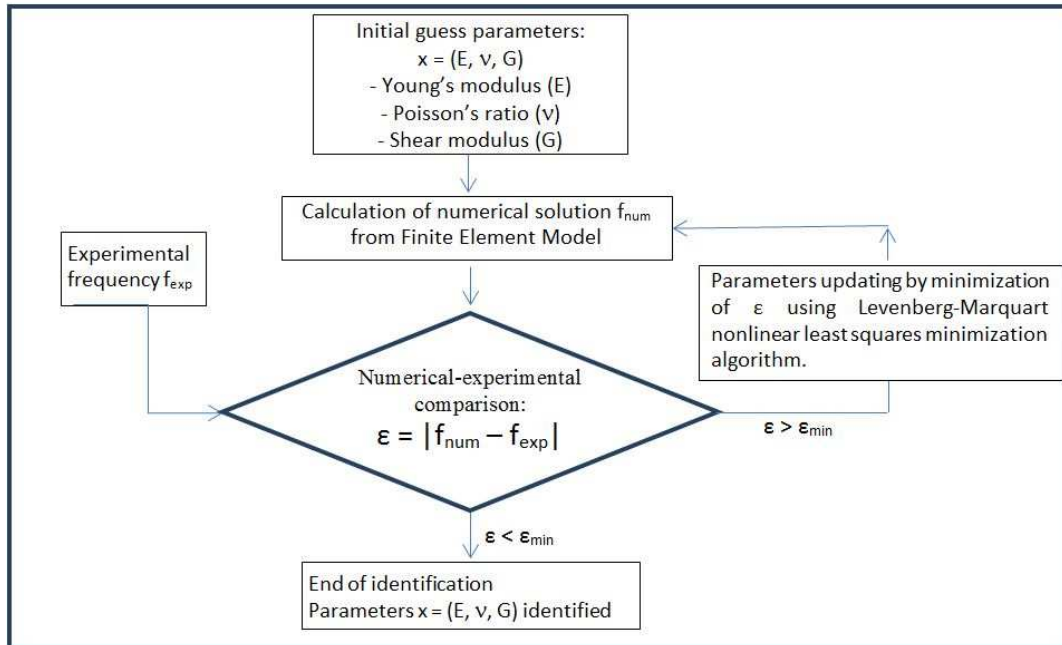
228 A frequency analysis of each beam specimen was performed in the FE software COMSOL.
229 Figure 7 shows the first three mode shapes that were analyzed. The COMSOL model
230 was assumed to be a homogeneous and isotropic beam.



231

232 **Figure 7 Modes 1, 2, and 3 of COMSOL beam model used for frequency analysis**

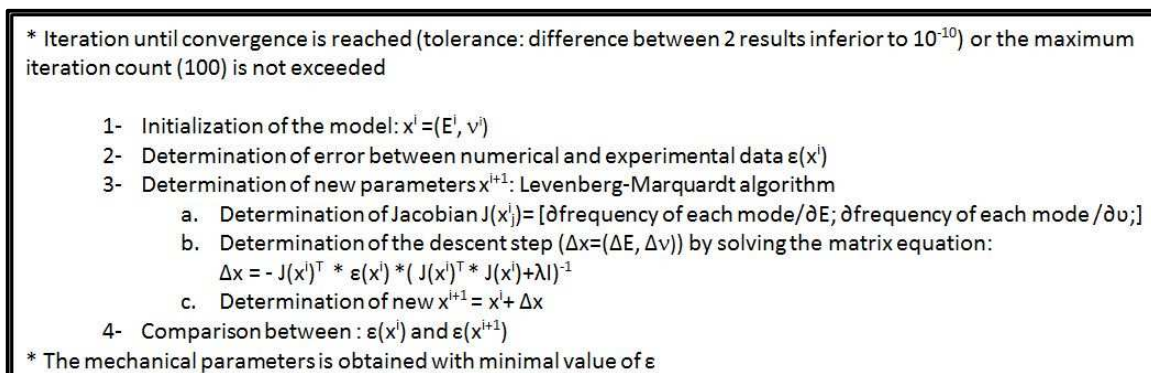
233 A custom application using COMSOL Java API has been developed so as to determine
 234 mechanical parameters, by using a mixed numerical-experimental identification method based
 235 on the modal response of samples of tilestone. This technique is founded on the minimization
 236 of the discrepancies between the eigenvalues computed with a3D finite element model with
 237 adjustable elastic properties and the corresponding experimental quantities(figure 8)[34,35].



238

239 **Figure 8 Principle of the iterative resolution of the inverse numerical problem of identification**

240 In order to maximize the quality of the identification, free-free boundary condition is chosen
 241 for the experimental determination of the eigenfrequencies. A classical Levenberg-Marquardt
 242 nonlinear least squares minimization algorithm is used to solve the inverse problem of finding
 243 the elastic constitutive parameters which best match the experimental modal data (Figure 9).



244

245 **Figure 9 Simplified Levenberg-Marquardt minimisation algorithm developed in JAVA in COMSOL API**

246 **3. Results and discussion:**

247 **3.1. Vibration damage monitoring of tilestone subject to freeze-thaw cycle:**

248 The first result of this study concerns frequency monitoring of tilestone subject to freeze-thaw
249 cycle and is shown on figure10. A variation of at least 5% is usually required to consider that
250 the structure has damaged[36]. We observe that (figure 10), for each sample cutfrom the same
251 stone, the sensitivity to weathering during freeze-thaw is not identicalbetweeneach mode. This
252 means that, frequency response is sensitive to different processes of weathering occurring in
253 different samples and different types of stone. Figure11 is a comparison of the mean of
254 $RDEM_i(n)$ of the three samples. As we can observe, there are 3 scenarios of frequency
255 responses. The first is associated to a negligible sensitivity on frequencies (stone M). In the
256 second scenario, not all the frequencies have the same sensitivity to weathering (stone L). In
257 the last scenario, all the frequencies are sensitive to weathering (stone S). These scenarios are
258 obviously a manifestation of damage occurring inside the structure at the meso and thus the
259 micro scale of each sample.

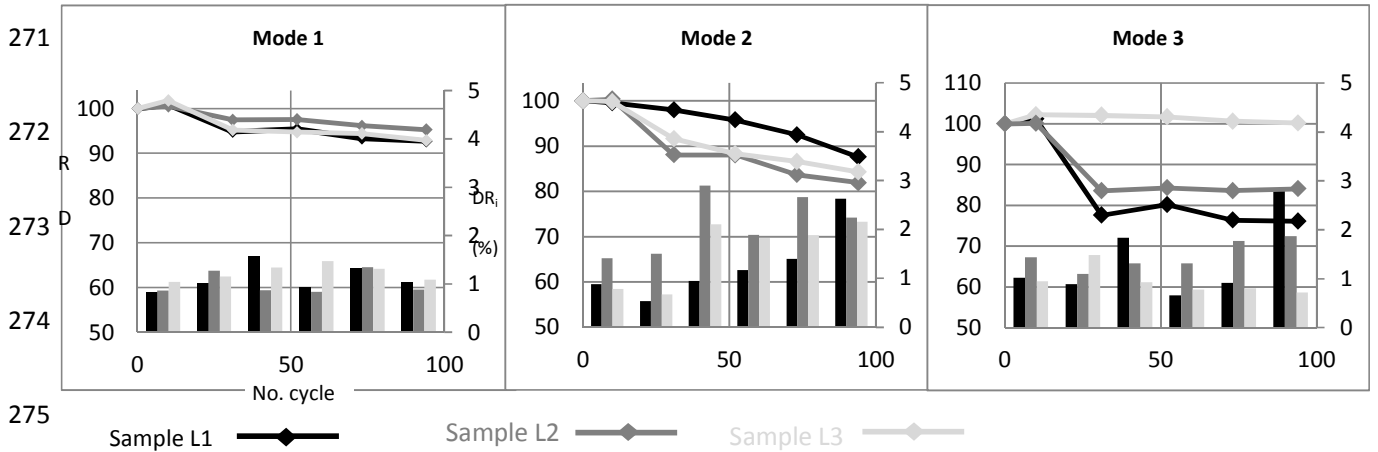
260 Besides, Figure 10 presents the evolution of the damping ratio (DR). Damping ratio mainly
261 increasedduring the freeze-thaw cycles, and this increase is higher for the modesthat exhibit
262 the higher decrease in frequency. The increase of the damping ratio, which is a measure of the
263 energy dissipation of a vibrating structure, is probably the consequence of the micro-frictions
264 of the cracks inducedin the samples during freeze-thaw cycles. Indeed, while the sensitive of
265 frequency indicates an eventual occurrenceof damage, damping is useful to revealthe
266 modeswhich are the most sensible to that damage. The sampleswhich show the highest
267 sensitivity on frequencies alsoexhibitthe highest damping ratio.

268

269

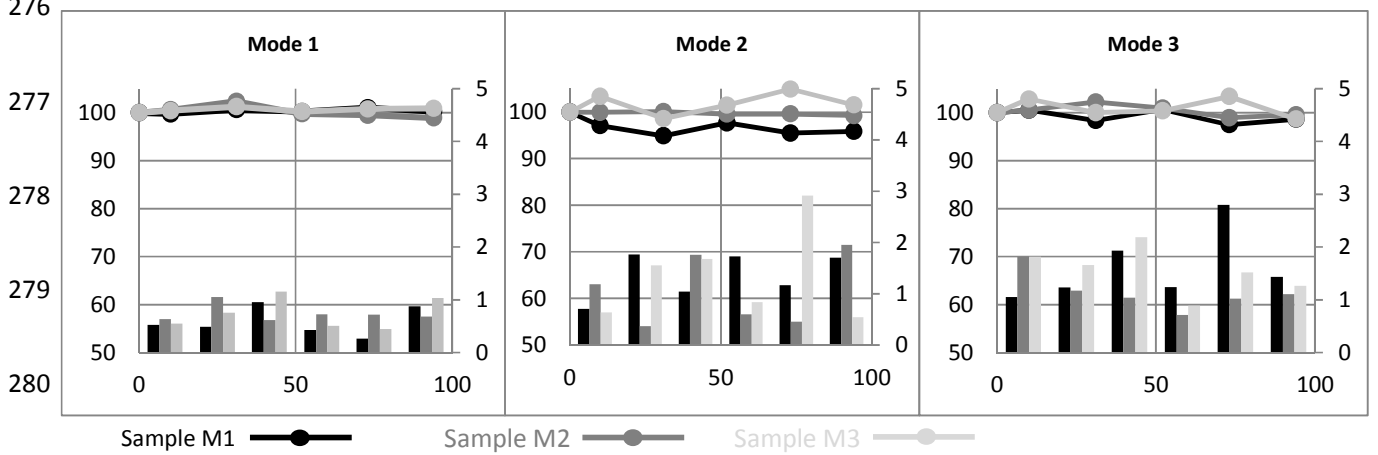
270

Stone L



275

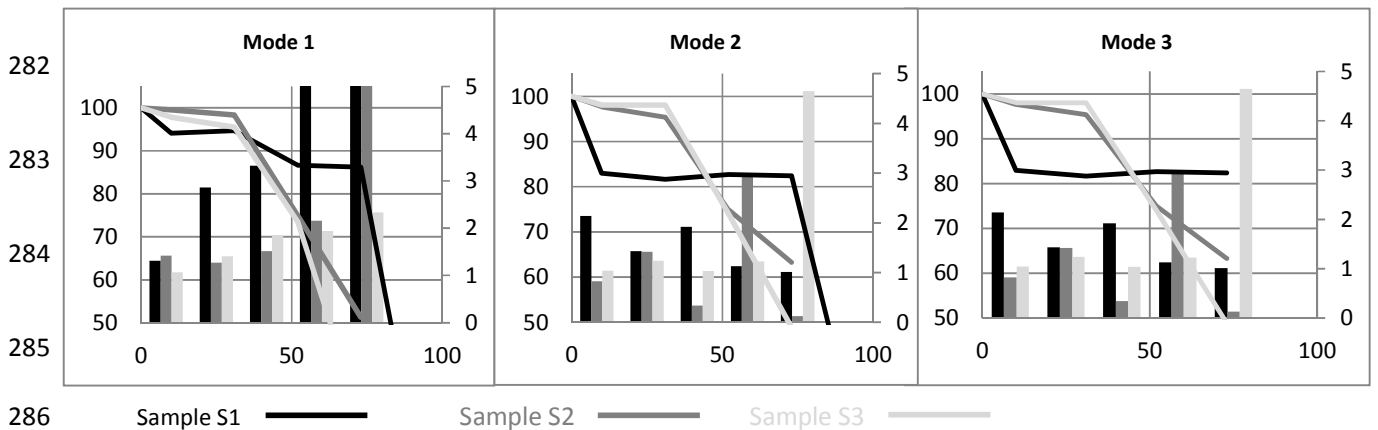
Stone M



278

281

Stone S



286

287 **Figure 4** Evolution of RDMEi (%) and DRi (%) during freeze-thaw cycles of different samples for the 3 first eigenmodes. RDMEi (%) is in solid line (left vertical axis) and DRi (%) is in bars (right vertical axis).

288

289

290

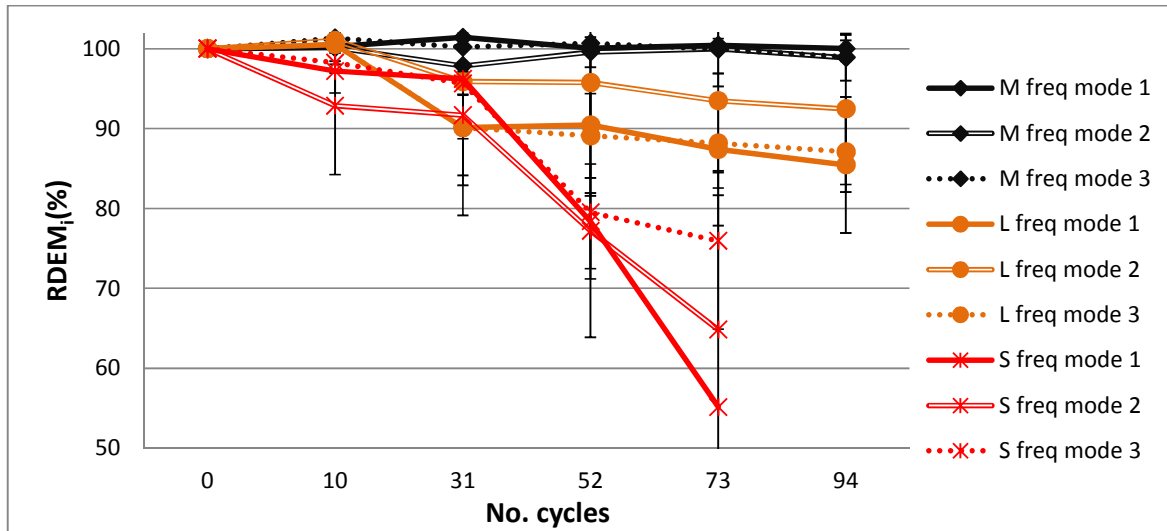


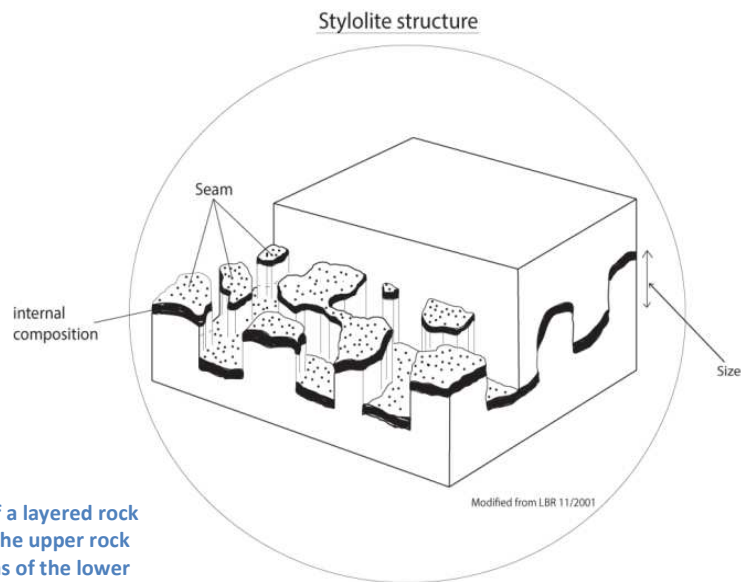
Figure 5 Evolution of RDMEi (%) of stone samples during freeze-thaw cycles

291

292 3.2. Relationship between macroscopic damage and micro/mesoscale structure

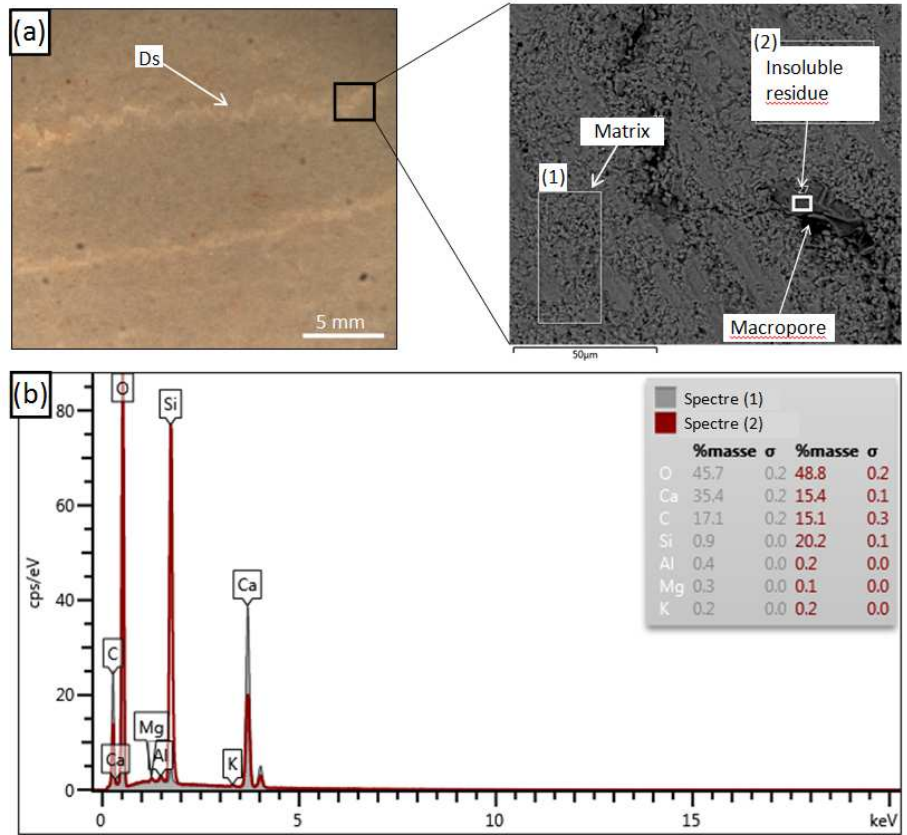
293 Vibration response allows assessing and monitoring damage that occurs in a stone submitted to
 294 a freeze thaw cycle. This damage is a manifestation of defects appearing in the structure
 295 because of the strain generated by the hygrothermal process occurring during the freeze / thaw
 296 cycles. According to the network characteristic of stones L and M, these stones are frost
 297 resistant. In fact, stone L and M have a unimodal porous network and consist essentially of
 298 micropores (about 13 nanometers for sample L and less than 7 nanometers for sample
 299 M). These poral characteristics make them have, either a difficult saturation, due to a poor
 300 capillarity, or a lower temperature of freezing due to the fineness of pore sizes. In fact, for a
 301 porous media of a few nanometers, the freezing temperature can be lowered to -80°C [37].
 302 However for samples of the stone S, the porous media is bimodal, and consists of a majority
 303 of mesoporous (between 100 nm and 1000 nm) and a few parts of micropores (figure 4). For
 304 pores of this size, water contained in the media can be frozen (freezing temperature for pore
 305 of $0,1\mu\text{m}$ diameter is -10°C [34]), generating strain inside the sample which can lead to
 306 damage, as has been observed (Figure 15). This strain can be caused either by the increasing
 307 of the water size, or the migration of water from the small sized pore to the large sized pore
 308 by cryosuction [12].

309 Although stone L is frost resistant, due to its porous characteristics, partial damage has been
310 observed through vibration response and at the mesoscale by the appearance of horizontal
311 cracks. A zoom on these damaged zones shows that damage occurred on pre-existent
312 diagenetic feature zones (Ds in Nicholson classification) called stylolite. This diagenetic
313 feature is due to a phenomenon of pressure dissolution occurring inside the rock during its
314 formation [38]. Stylolite is characterized by its size and its internal composition, which is
315 insoluble (figure 12). This diagenetic feature is often encountered in limestone bedrock.
316 Stylolite has been shown as being a zone of weakness since the porosity in the vicinity of this
317 diagenetic feature is always higher than that of the host rock, and further there is a significant
318 strength reduction expected with the presence of a stylolite in a stone, even when thin and
319 closed [39].



320
321
322
323
324
325 **Figure 6 Three-dimensional block diagram of a layered rock with a horizontal stylolite. The front half of the upper rock mass has been removed to show the columns of the lower block [40]**
326

327 MEB and microscopic observation and investigation on this pre-existing diagenetic feature
328 zone where the damage has occurred reveal that, on sample L and sample S, Ds is either a
329 zigzag or a wavy sutured zone with macropores (around 5 μm of diameter), and inside it is
330 possible to find insoluble siliceous residue (Figure 13). These macropores were not identified
331 with mercury porosity measurements.

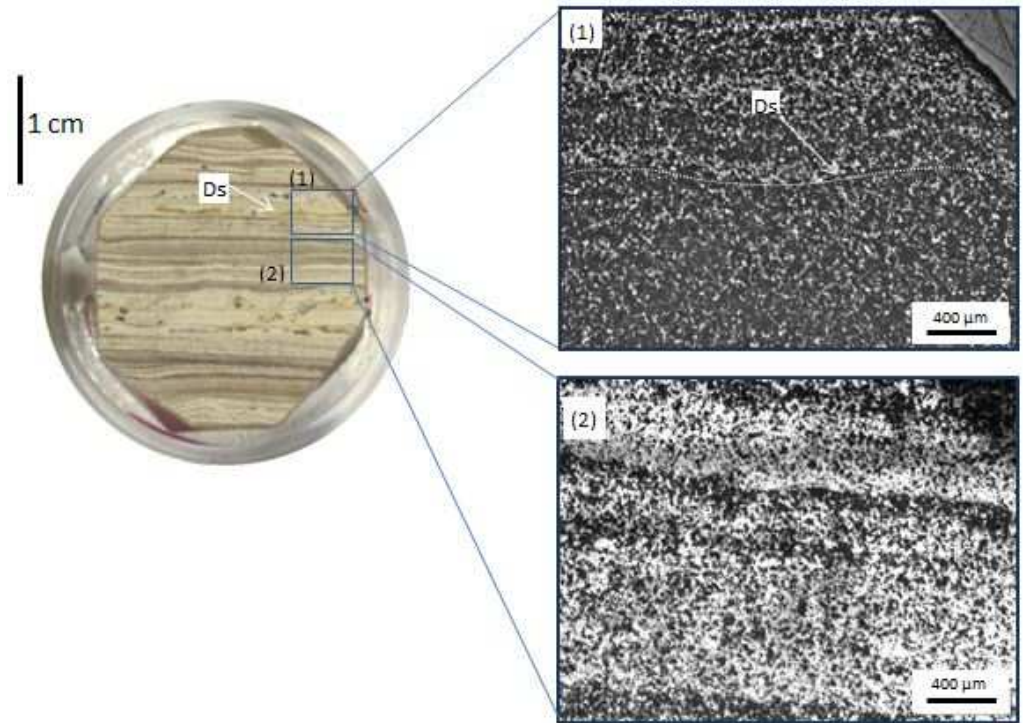


332

333

334

Figure 13 (a) Stylolite (Ds) SEM BSE observation of stone L, (b) Chemical analysis comparison of matrix and the siliceous insoluble residue inside the stylolite (Ds). Ds and its vicinity are porous zones-, and it contains siliceous insoluble residue.



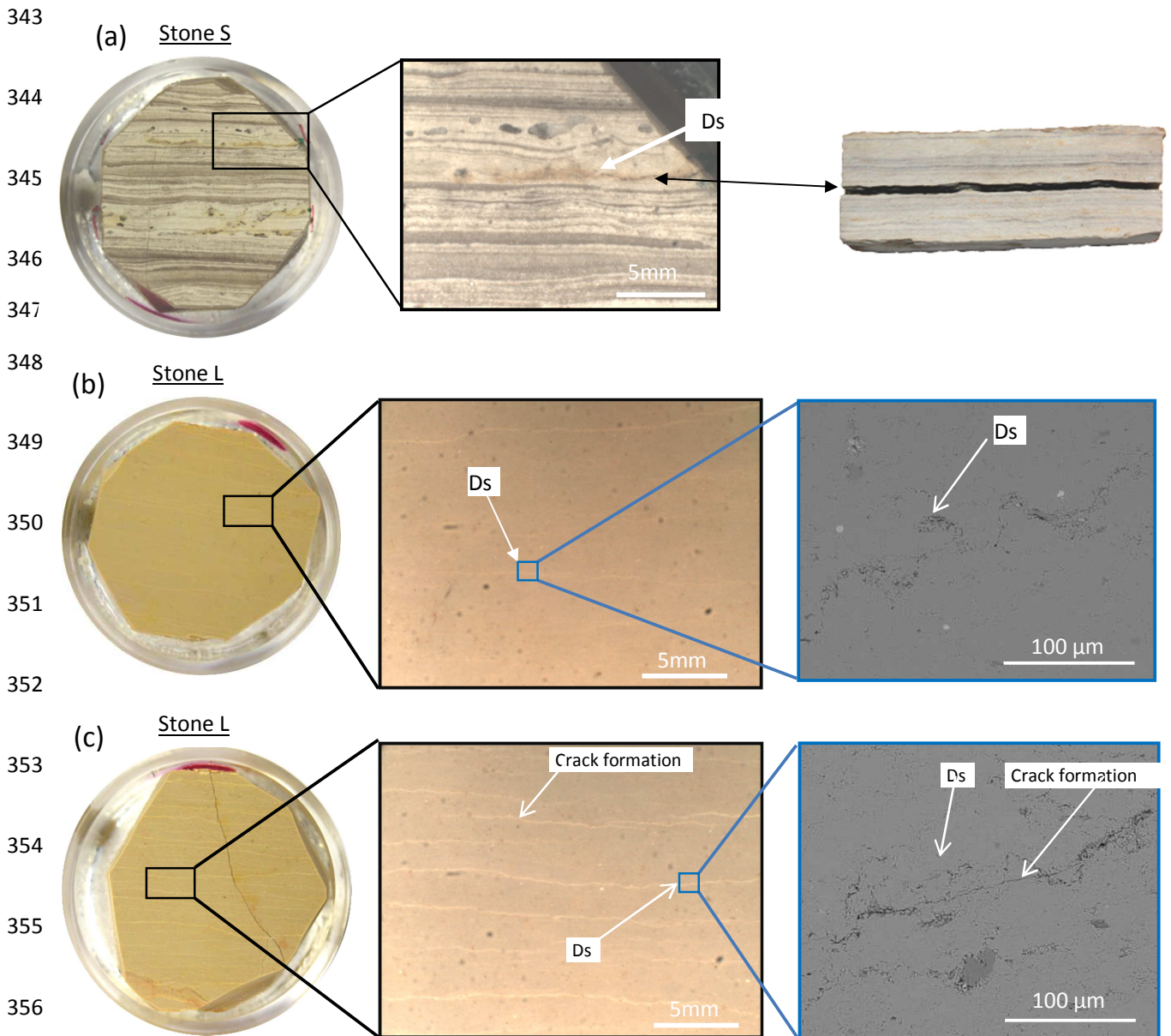
335

336

337

Figure 14 Microscopic observation of flaw zone of stone S. The contrast of porosity is expressed by the gray level contrast. Ds is located among a highly porous zone (1), then it is weaker than zone (2)

338 The difference between stylolite in samples S and L is the ratio and the size of the porous
 339 zone in its vicinity. As observed on Figure 14, the contrast of gray level proves that
 340 the diagenetic feature zone in sample S is more porous (around 5 μm for sample L and around
 341 100 μm for sample S) and thus makes it less resistant and more vulnerable to hydrothermal
 342 process occurring during the freeze-thaw cycle (Figure 15)



357 **Figure 15 SEM BSE and optical microscope images comparison obtained from pre-existing diagenetic feature of sample S and sample L**
 before and after freeze-thaw cycle at meso and micro scale. (a) Sample S break at pre-existing diagenetic feature (b) Pre-existing
 diagenetic features (Ds) exist and it is not very visible. (c) After freeze-thaw cycle cracks appear in the zone where there are pre-existing
 358 diagenetic features.

359 **3.2 Discussion on the mechanical properties:**

360 Table 3 below presents the mechanical parameters of each tilestone at their initial state and
 361 after 94 cycles, determined by using a mixed numerical-experimental identification method
 362 based on the modal response of samples of tilestone.

363 Table 3: Comparison of mechanical parameters before and after freeze-thaw cycles
 364

Mechanicals parameters		Stone L	Stone M	Stone S
E (GPa)	Before	61,88 (+/- 0,65)	63,98 (+/-1,98)	64,38 (+/-2,1)
	After	60,56 (+/- 1,12)	63,29 (+/- 1,66)	37,16
Evolution of Young's modulus		- 2%	- 1%	- 42%
G (GPa)	Before	24,24 (+/- 0,31)	25,17 (+/- 0,48)	25,85 (+/-0,39)
	After	20,84 (+/- 0,81)	24,85 (+/- 0,74)	14,77
Evolution of Shear Modulus		- 14 %	-1,3 %	- 43 %

365
 366 As expected, there is a reduction of Young and shear modulus after the 94 cycles for damaged
 367 samples. Sample S presents a reduction of Young and shear modulus of about - 42 % at the
 368 end of the cycles. These values are consistent to those used in the case of concrete which is
 369 40% [22] for damaged specimens. In addition, we observed that for samples with partial
 370 damage (Sample L), the shear modulus decreased more than the Young modulus. This
 371 phenomenon is consistent with the process of damage occurring in this sample. In fact the
 372 existence of a horizontal crack indicates that the rock has undergone shear damage.

373

374

375

376

377 **4. Conclusions**

378 This study investigates the freeze-thaw resistance of limestone roofing stone, selected from the
379 last remaining active quarries in the southern region of the Massif Central, through a method
380 based on the vibration response of the structure. The ongoing damage induced by freeze-thaw
381 cycles was quantified from the loss of stiffness, obtained by FE model updating
382 techniques, and the increase of damping monitored from the vibration response of beam
383 samples. The main conclusions from the study can be summarized as follows:

384 1) Monitoring of frequency and damping ratio is actually efficient to measure damage
385 occurring during the freeze-thaw cycle: while frequency monitoring allows assessing
386 the occurrence of damage, damping ratio informs on its severity in the structure. The
387 use of mixed numerical-experimental identification method applied on isotropic FE
388 model, to assess dynamic mechanical parameters and damage, is effective.

389 2) Limestone tilestone with unimodal porous media consisting of essentially micropore
390 are more frost resistant than limestone tilestone with bimodal porous media consisting
391 of partially mesopore. However, presence of pre-existing diagenetic features, such as
392 stylolites (Ds in Nicholson classification), inside limestone tilestone with unimodal
393 micropore, or with presence of high porosity volume, constitute weaknesses of the
394 stone that can lead to damage.

395 Further investigations will concern on the one hand, the characterization of the damaging
396 process occurring in this material by comparing the influence of thermal and hydric process,
397 and on the other hand the improvement of the FEM (Finite Element Model)-based identification
398 strategy, in order to account for the possible anisotropy of the stone structure induced by its
399 sedimentary formation and possibly increased by the occurrence of local damage.

400

401

402 **Funding**

403 This research is a part of the project LAUBAMAC financed by CGET of the Massif Central
404 in France.

405 **Acknowledgements**

406 The authors would like to acknowledge the tilestone quarries(Montdardier, SAS Lauzas,
407 ALLA) for making available the samples that enabled us to conduct this study. The authors
408 also wish to express their sincere appreciation toChristian Buisson, engineer, and Cathie
409 O'Neill, director of the ABPSassociation and coordinator of the LAUBAMACproject,for their
410 assistance in this work.

411 **Bibliography:**

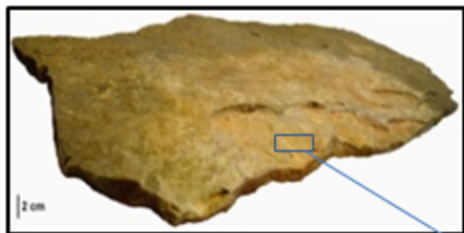
- 412 [1] E.A. Laycock, D. Jefferson, S. Hetherington, F. Clegg, C. Wood, Revitalising
413 Collyweston limestone slate production by artificial freeze/thaw splitting, *Constr.*
414 *Build. Mater.* 159 (2018) 486–498. doi:10.1016/j.conbuildmat.2017.10.039.
- 415 [2] V. Cárdenes, Á. Rubio-Ordóñez, J. Wichert, J.P. Cnudde, V. Cnudde, Petrography of
416 roofing slates, *Earth-Science Rev.* 138 (2014) 435–453.
417 doi:10.1016/j.earscirev.2014.07.003.
- 418 [3] J.P. Ingham, Roofing slate, *Geomaterials Under Microsc.* (2013) p.51-60.
- 419 [4] N.H.M. Swinburne, C. Hemleben, The Plattenkalk facies : a deposit of several
420 environments., *GEOBIOS.* (1994) 313–320.
- 421 [5] V. Cárdenes, Á. Rubio-Ordóñez, C. Monterroso, F.J. Mateos, Guidelines for selecting
422 roofing slate for the restoration of historical buildings and monuments: two case
423 studies, *J. Cult. Herit.* 15 (2014) 203–208. doi:10.1016/j.culher.2013.02.004.
- 424 [6] C. Walbert, J. Eslami, A.-L. Beaucour, A. Bourges, A. Noumouwe, Evolution of the
425 mechanical behaviour of limestone subjected to freeze thaw cycles, *Environ. Earth Sci.*
426 (2015) 6339–6351.
- 427 [7] J. Eslami, C. Walbert, A.L. Beaucour, A. Bourges, A. Noumowe, Influence of physical
428 and mechanical properties on the durability of limestone subjected to freeze-thaw

- 429 cycles, *Constr. Build. Mater.* 162 (2018) 420–429.
430 doi:10.1016/j.conbuildmat.2017.12.031.
- 431 [8] E. Flugel, *Microfacies of Carbonate Rocks. Analysis, Interpretation and Application*,
432 Berlin, Heidelberg, New York: Springer-Verlag, 2004. doi:10.1007/978-3-662-08726-
433 8.
- 434 [9] D.T. Nicholson, F.H. Nicholson, Physical deterioration of sedimentary rocks subjected
435 to experimental freeze-thaw weathering, *Earth Surf. Process. Landforms.* 25 (2000)
436 1295–1307. doi:10.1002/1096-9837(200011)25:12<1295::AID-ESP138>3.0.CO;2-E.
- 437 [10] PRICK Angélique, Critical Degree of saturation as a Threshold Moisture Level in Frost
438 Weathering of Limestones, *Permafr. Periglac. Process.* 8 (1997) 91–99.
- 439 [11] T.C. Chen, M.R. Yeung, N. Mori, Effect of water saturation on deterioration of welded
440 tuff due to freeze-thaw action, *Cold Reg. Sci. Technol.* 38 (2004) 127–136.
441 doi:10.1016/j.coldregions.2003.10.001.
- 442 [12] M. Bellanger, F. Homand, J.M. Remy, Water behavior in limestones as a function of
443 pore structure: application to frost resistance of some lorraine limestones., *Eng. Geol.*
444 36 (1993) 99–108.
- 445 [13] A. Saad, S. Guedon, F. Martineau, Microstructural weathering of sedimentary rocks by
446 freeze-thaw cycles: Experimental study of state and transfer parameters., *Comptes*
447 *Rendus Geosci.* (2010) 197–203.
- 448 [14] Walbert Charlotte, Eslami Javad, Beaucour Anne-Lise, Bourges Ann, A. Noumouwe,
449 Evolution of the mechanical behaviour of limestone subjected to freeze thaw cycles,
450 *Env. Earth Sci.* (2015) 6339–6351.
- 451 [15] J. Martínez-Martínez, D. Benavente, M. Gomez-Heras, L. Marco-Castaño, M.Á.
452 García-Del-Cura, Non-linear decay of building stones during freeze-thaw weathering
453 processes, *Constr. Build. Mater.* 38 (2013) 443–454.
454 doi:10.1016/j.conbuildmat.2012.07.059.

- 455 [16] A. Saad, Influence du changement climatique et des conditions extrêmes sur les
456 massifs fracturés : rôle des fluides dans leur processus d'altération, 2011.
- 457 [17] B. Christaras, F. Auger, E. Mosse, Determination of the moduli of elasticity of rocks.
458 Comparison of the ultrasonic velocity and mechanical resonance frequency methods
459 with direct static methods, *Mater. Struct.* 27 (1994) 222–228.
460 doi:10.1007/BF02473036.
- 461 [18] R.J. Allison, A non-destructive method of determining rock strength, *Earth Surf.*
462 *Process. Landforms.* 13 (1988) 729–736. doi:10.1002/esp.3290130807.
- 463 [19] A. Saad, M. Bost, The resonant frequency measurement and cracking evolution in
464 rocks, *Rock Eng. Difficult Gr. Cond. - Soft Rocks Karst - Proc. Reg. Symp. Int. Soc.*
465 *Rock Mech. EUROCK 2009.* (2010) 345–350.
- 466 [20] H. Wu, Z. Liu, B. Sun, J. Yin, Experimental investigation on freeze-thaw durability of
467 Portland cement pervious concrete (PCPC), *Constr. Build. Mater.* 117 (2016) 63–71.
468 doi:10.1016/j.conbuildmat.2016.04.130.
- 469 [21] F. Matakah, P. Soroushian, Freeze thaw and deicer salt scaling resistance of concrete
470 prepared with alkali aluminosilicate cement, *Constr. Build. Mater.* 163 (2018) 200–
471 213. doi:10.1016/j.conbuildmat.2017.12.119.
- 472 [22] M.S.M. Lund, K.K. Hansen, R. Brincker, A.H. Jensen, S.D.R. Amador, Evaluation of
473 freeze-thaw durability of pervious concrete by use of operational modal analysis, *Cem.*
474 *Concr. Res.* 106 (2018) 57–64. doi:10.1016/j.cemconres.2018.01.021.
- 475 [23] R. Brincker, C. Ventura, *Introduction to Operational Modal Analysis*, Wiley-
476 Blackwell; 1 edition, 2015.
- 477 [24] M.S. Cao, G.G. Sha, Y.F. Gao, W. Ostachowicz, Structural damage identification using
478 damping: A compendium of uses and features, *Smart Mater. Struct.* 26 (2017).
479 doi:10.1088/1361-665X/aa550a.
- 480 [25] Shahzad S, Detection of corrosion-induced damage in reinforced concrete beams based

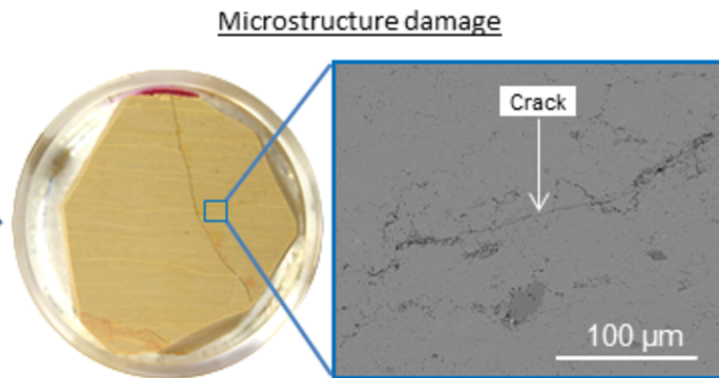
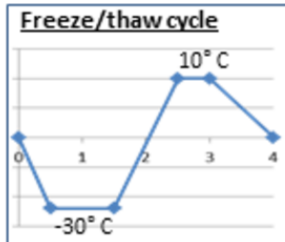
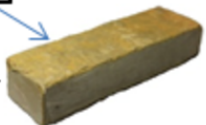
- 481 on structural damping identification, in: Proc. 13th East Asia-Pacific Conf. Struct. Eng.
482 Constr. G-2-4, n.d.: p. 2013.
- 483 [26] C. Modena, D. Sonda, D. Zonta, Damage Localization in Reinforced Concrete
484 Structures by Using Damping Measurements, Key Eng. Mater. 167–168 (1999) 132–
485 141. doi:10.4028/www.scientific.net/KEM.167-168.132.
- 486 [27] Y. Bodeur, The Upper Jurassic lithographic limestones of the Causse de Blandas-
487 Montdardier (Languedoc, France) in their palaeostructural framework, GEOBIOS. 16
488 (1994) 219–225.
- 489 [28] SCIAU Jacques, Dans les pas des Dinausaures des Causses : Inventaires des sites à
490 empreintes, Association Paléontologique des Causses, 2003.
- 491 [29] AFNOR, NF EN 1936 Méthodes d’essai des pierres naturelles - Détermination des
492 masses volumiques réelle et apparente et des porosités ouvertes et totale, n.d.
- 493 [30] European Committee for Standardization, EN 12371 Natural Stone tests methods:
494 determination of frost resistance, Bruxelles, 1966.
- 495 [31] S. Corn, P. Ienny, J.S. Dupuy, L. Daridon, Identification des propriétés viscoélastique
496 d’un PMMA par analyse vibratoire : comparaison entre différentes méthodes
497 expérimentales Abstract :, Cfm. (2009) 24–28.
- 498 [32] J.D. Ewins, Modal Testing: Theory, Practice and Applications, Research Studies Pr,
499 1984.
- 500 [33] T.J. Chalko, N. Haritos, V. Gershkovich, Non-linear curve fitting for modal analysis,
501 Environ. Softw. 11 (1996) 9–18. doi:http://dx.doi.org/10.1016/S0266-9838(96)00016-
502 0.
- 503 [34] J. Cugnoni, Identification par recalage modal et fréquentiel des propriétés constitutives
504 de coques en matériaux composites, (2005) 251.
- 505 [35] T. Lauwagie, H. Sol, G. Roebben, W. Heylen, Y. Shi, O. Van der Biest, Mixed
506 numerical-experimental identification of elastic properties of orthotropic metal plates,

- 507 NDT E Int. 36 (2003) 487–495. doi:10.1016/S0963-8695(03)00048-3.
- 508 [36] O.S. Salawu, Detection of structural damage through changes in frequency: a review,
509 Eng. Struct. 19 (1997) 718–723. doi:10.1016/S0141-0296(96)00149-6.
- 510 [37] A.B. Harnik, U. Meier, A. Rosw, Combined Influence of Freezing and Delcing Salt on
511 Concrete—Physical Aspects, Durab. Build. Mater. Components. ASTMSTP 69 (1980)
512 474–484.
- 513 [38] F. Renard, Three-dimensional roughness of stylolites in limestones, J. Geophys. Res.
514 109 (2004) B03209. doi:10.1029/2003JB002555.
- 515 [39] P. Baud, A. Rolland, M. Heap, T. Xu, M. Nicolé, T. Ferrand, T. Reuschlé, R.
516 Toussaint, N. Conil, Impact of stylolites on the mechanical strength of limestone,
517 Tectonophysics. 690 (2016) 4–20. doi:10.1016/j.tecto.2016.03.004.
- 518 [40] L. Bruce Railsback, An Atlas of Pressure Dissolution Features, (2001).

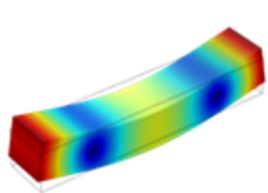


Tilestone

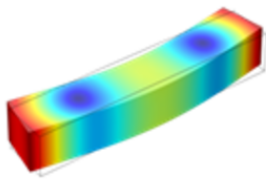
parallelepiped sampling



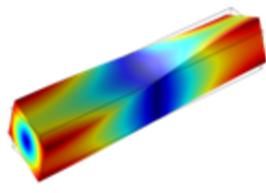
Damage Monitoring based on vibration measurements and FE modeling



Mode 1: bending



Mode 2: bending



Mode 3: torsion

